Inclusive α-production cross section for the ^{6}Li + ^{90}Zr system at energies near the fusion barrier

H. Kumawat,* V. Jha,† V. V. Parkar,‡ B. J. Roy, S. Santra, V. Kumar, D. Dutta, P. Shukla, L. M. Pant, A. K. Mohanty, R. K. Choudhury, and S. Kailas

Nuclear Physics Division, Bhabha Atomic Research Centre, Mumbai 400085, India

(Received 11 January 2010; revised manuscript received 26 February 2010; published 17 May 2010)

Inclusive (direct + compound) α production for the ^{6}Li + ^{90}Zr system is measured at near barrier energies, namely, 15, 17, 19, 21, 25, and 30 MeV. The data are treated in the statistical model and distorted-wave Born approximation framework to disentangle the degree of competition between direct and compound reaction channels. A substantial contribution from the compound reaction channels is obtained but the direct reaction channels are found to be the dominant mechanism for α production at these energies. Estimation of the breakup and transfer reaction around the barrier shows that the latter is the dominant channel. Universal behavior of the α-production cross section is observed over a large range of target nuclei.

DOI: 10.1103/PhysRevC.81.054601 PACS number(s): 25.70.Bc, 25.70.Mn, 25.70.Hi, 25.70.Ef

I. INTRODUCTION

The coupling of collective and internal degrees of freedom to the relative kinetic energy in heavy-ion reactions plays an important role at around the Coulomb barrier and is manifested by (i) an enhancement or suppression of the fusion cross section [1–6] and (ii) a threshold anomaly [7–19] in the optical potential. Sub-barrier fusion cross sections are generally found to be enhanced compared to the one-dimensional barrier penetration model. This is explained in terms of couplings to inelastic excitations of the projectile or target and transfer channels. In the case of reactions where loosely bound projectiles are involved, breakup becomes one of the important reaction channels. Different reaction channels have not yet been clearly identified either in exclusive or inclusive measurements or by theoretical estimation of the individual reaction channels to obtain a systematic understanding of the inclusive data. However, there have been conflicting experimental results [2,6,20] and theoretical interpretations [21–24] regarding suppression or enhancement of fusion cross sections compared with coupled-channel calculations in case of loosely bound nuclei. Interest in the loosely bound nuclei has renewed with the recently available radioactive ion beams.

In general, coupling to inelastic and transfer channels will enhance the possibility of fusion, and breakup may suppress it owing to only partial fusion of some of the projectile fragments. Because of the low breakup threshold in the case of loosely bound nuclei, the dynamics of the reaction channels is affected and there may be loss of flux owing to projectile breakup in the nuclear and Coulomb fields before fusion takes place. Generally, experimental data seem to indicate that the magnitude of suppression in complete fusion above the barrier may be consistent with the yield of incomplete fusion [1]. However, there is a limited understanding of enhancement behavior of fusion at below-barrier energies for weakly bound or exotic nuclei. In our previous systematic study [25] of ^{6}Li, it was observed that nuclear breakup dominates the breakup mechanism for various target nuclei.

Inclusive and exclusive α measurements suggest [12,26–28] that the large α production is connected to the transfer and breakup channels. Recent studies [29,30] reveal that exclusive breakup and compound nuclear processes contribute only 10% and 30% to the total α production. More experimental data are required to clarify this problem.

In the present work, we report measurements of the inclusive α angular distributions for the ^{6}Li + ^{90}Zr system at near-barrier energies to enlighten these aspects further. The ^{90}Zr target nucleus is a spherical neutron magic nucleus and the first excited state (1.760 MeV) is above the ^{6}Li breakup threshold (1.475 MeV), therefore target inelastic couplings do not play an important role. Dominant contributions from couplings to the breakup and transfer channels are expected. Statistical model calculations using PACE [31] are performed to estimate the compound nuclear reaction contributions. We also report distorted-wave Born approximation (DWBA) calculations for studies of n- and p-transfer reactions for the ^{6}Li + ^{90}Zr system contributing to α production through $^{6}\mathrm{Li} \rightarrow {}^{5}\mathrm{Li} + n \rightarrow {}^{4}\mathrm{He} + p + n$ and $^{6}\mathrm{Li} \rightarrow {}^{5}\mathrm{He} + p \rightarrow {}^{4}\mathrm{He} + n + p$, respectively.

The outline of this paper is as follows. In Sec. II, we present experimental details. Section III reports the analysis procedure used to extract the experimental data. Section IV describes the statistical model calculations. In Sec. V, DWBA calculations for studies of n- and p-transfer coupling effects for the ^{6}Li + ^{90}Zr system are presented. Section VI includes discussion and comparison with previously studied systems. Conclusions are drawn in Sec. VII.

II. EXPERIMENTAL DETAILS

A detailed description of the experimental setup is given in a previous study [25] and only a short summary pertinent to this work is mentioned here. Measurements were performed using the $^{6}\mathrm{Li}^{3+}$ beam delivered by the 14UD Pelletron accelerator

*harphool@barc.gov.in

†Present address: IKP, Forschungszentrum, Jüelich, D-52425, Germany; v.jha@fz-juelich.de

‡Present address: DNAP, Tata Institute of Fundamental Research, Mumbai 400005, India.

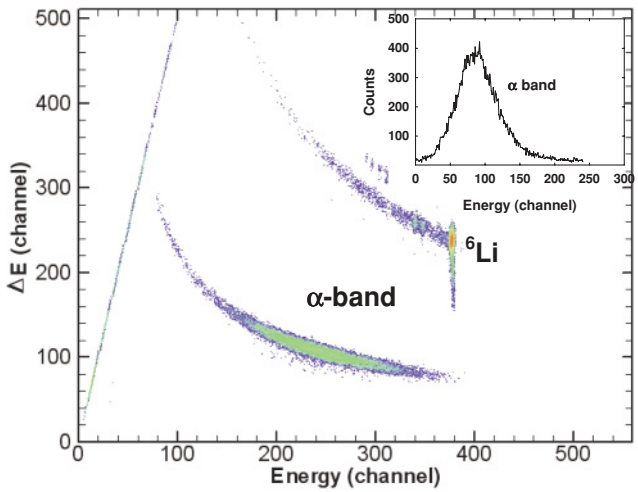

FIG. 1. (Color online) $\Delta E - E$ two-dimensional spectra at 30 MeV, $\theta = 55^\circ$, for the ^{6}Li + ^{90}Zr system. The α band is projected in the inset.

at the Bhabha Atomic Research Centre (BARC)/Tata Institute of Fundamental Research (TIFR) Facility in Mumbai, India, at bombarding energies of 15, 17, 19, 21, 25, and 30 MeV with beam intensities of 5–30 *pn*A. The beam impinged on a 400 μg/cm^2, self-supported, enriched ($\geqslant$99%) ^{90}Zr target. Beam energies were corrected for energy loss in a half-target thickness during the analysis process. Charged particles were detected by four solid-state silicon surface barrier detectors in the $\Delta E + E$ telescopic arrangement. The α group was well discriminated from other products, as shown in Fig. 1. Proton and deuteron bands are not observed owing to the detector threshold. In the inset, the projection of the α band is shown, which is nearly Gaussian in shape. A monitor detector 1000 μm thick was mounted at 22° for absolute cross-section normalization. Angular distributions were measured at angles of from 25° to 173° at lower energies and from 25° to 100° at higher energies. Statistical errors in the data were less than 1% at grazing angles and a maximum of 5% at backward angles.

III. EXPERIMENTAL RESULTS

As mentioned previously, α particles were well resolved or identified in the setup. Typical energy spectra of α particles at three angles for 30 MeV along with the statistical model predictions are shown in Fig. 2. The maximum yield of α particles was observed at the α-particle energy, where the kinetic energy per nucleon is equivalent for the α particle and the projectile. From the spectral anisotropy, it is clear that the spectra include the evaporation as well as the direct contributions. At higher energies, the backward-angle contribution comes mostly from the compound nuclear reactions. The spectra are of Gaussian shape and the small tails at low energy are attributed to several processes, such as (i) decay of the incomplete fusion and transfer residues, (ii) reactions with carbon deposited on the target during irradiation, and (iii) reactions with the oxidized target layer. The evaporation peak (3 MeV) from the ^{6}Li + ^{12}C compound is below the ΔE

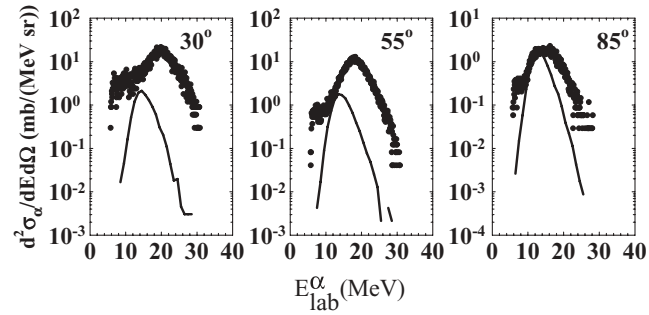

FIG. 2. Energy spectra of the α groups in the reaction ^{6}Li + ^{90}Zr at 30 MeV at various angles. Experimental inclusive and calculated compound portions are designated by filled circles and lines, respectively. Backward-angle spectra are constituted almost exclusively of the compound portion.

detector threshold (3.5–5 MeV), thus we could not see this peak in any of the two-dimensional (2-D) spectra. Another possibility is that the α particles are from the oxidized Zr layer. The α-particle peak from evaporation of ^{6}Li + ^{16}O is also in a similar energy range. It was difficult to separate the carbon and oxygen contaminations. The total contamination was estimated by fitting the tail of the α-particle spectra, which was exponential in nature. In this procedure we also obtained help from the 1-D spectra. At each angle, the integrated yields of the spectra were determined. The lower limit of the α energy is assumed to be 6 MeV in the integration procedure, which is above the estimated evaporation tail for the ^{90}Zr target obtained using the statistical model code PACE. The carbon and oxygen contamination together is estimated to be ~1% at 30 MeV (last energy of irradiation in the experiment) and it increases to ~2% at 25 MeV (last energy of irradiation in the experiment). We subtracted this contribution from the total α production. If we assume that the contamination is only from carbon, then its thickness is estimated to be ~3 μg/cm^2 at 30 MeV, which increases to ~6 μg/cm^2 at 25 MeV. The energy integrated angular differential cross section $d\sigma_\alpha^{\rm incl}/d\Omega$ was deduced using the following equation:

$$\frac{d\sigma_\alpha^{\rm incl}}{d\Omega} = \frac{Y_\alpha^{\rm incl}}{Y_{\rm el}} \frac{d\sigma_{\rm el}}{d\Omega}, \tag{1}$$

where $d\sigma_{\rm el}/d\Omega$ is the elastic scattering cross section obtained from the previous measurement [25], and $Y_\alpha^{\rm incl}$, and $Y_{\rm el}$ are the yields of α and elastic scattering, respectively. As the measurements were carried out up to extreme backward angles, the angle integrated (total α-production) cross sections could be extracted by fitting the differential angular cross sections along with a χ^2 minimization procedure. The shapes of the spectra below 25° were assumed to be similar to those estimated by continuum discretized coupled-channels (CDCC) calculations. Thus, the total α cross section was calculated using Eq. (2) at each energy as

$$\sigma_\alpha^{\rm incl} = \int_0^{2\pi} d\phi \int_0^{\pi} \frac{d\sigma_\alpha^{\rm incl}(\theta)}{d\Omega} \sin\theta d\theta. \tag{2}$$

The statistical error, which was up to 5% for angles far from the grazing angles, will cause only a small error in the total error, owing to $\sin\theta$ weighting. The error caused by the

TABLE I. Experimental α-production cross section ($\sigma_\alpha^{\text{incl}}$) deduced from the integral of the measured angular distributions, reaction cross section (σ_R) obtained from elastic scattering measurement [25], compound nuclear contribution (σ_{PACE}) simulated with the statistical model code PACE [31], and breakup ($\sigma_{\alpha+d}$), $1n$-transfer (σ_{1n}), and $1p$-transfer (σ_{1p}) cross sections from DWBA calculations.

E_{lab} (MeV)	$\sigma_\alpha^{\text{incl}}$ (mb)	σ_R (mb)	σ_{PACE} (mb)	$\sigma_{\alpha+d}$ (mb)	σ_{1n} (mb)	σ_{1p} (mb)
14.89	32 ± 19	42	0.1	8.5	8.8	1.4
16.90	122 ± 10	171	0.7	12.9	31.6	4.2
18.90	274 ± 15	417	6	17.9	61.3	7.3
20.91	360 ± 20	665	25	24.4	71.8	8.3
24.92	460 ± 30	1062	62	35.0	73.2	9.3
29.93	540 ± 86	1398	117	45.3	56.4	7.5

fitting procedure is weighted error with goodness of fits. The χ^2 values were varied from 0.7 to 1 for error estimation, with a 95% confidence limit. The total errors shown are the statistical and fitting errors. The derived experimental total α cross sections along with the errors are reported in Table I.

IV. THEORETICAL ANALYSIS: STATISTICAL MODEL CALCULATIONS

The α-production cross section from the compound reaction mechanism was estimated using the statistical model code PACE [31]. The excitation energy dependence of the level density parameter ($A/10$) was used according to the prescription of Ignatyuk *et al.* [32]. The compound nuclear spin distributions and fusion cross sections were obtained from CDCC calculations [25] where breakup coupling effects have been taken into account. The α-particle differential angular cross sections at different energies are given in Fig. 3. The angular distributions are isotropic in the center-of-mass frame. The cross section seems to be purely from the compound reaction channels at the higher projectile energies and well above the grazing angles. The calculated compound part is significantly less compared to the total α production near or below barrier energies, which indicates that other reaction channels such as transfer and breakup are the dominant processes at these energies. The direct reaction part is plotted after subtracting the compound nucleus contribution from the measured total α-production cross section.

V. THEORETICAL ANALYSIS: DISTORTED-WAVE BORN APPROXIMATION CALCULATIONS

The α-particle emission via direct reactions can be attributed to several mechanisms: (a) breakup [$^6\text{Li} \rightarrow \alpha + d(p+n)$], (b) d transfer ($Q = +9.3$ MeV), (c) n transfer ($Q = 1.5$ MeV), and (d) p transfer ($Q = 0.57$ MeV). We have performed the finite-range (DWBA) calculation owing to n and p transfers only. We have not considered the d transfer leading to states in the final nucleus ^{92}Nb, because, owing to the very high Q value (+9.3 MeV), it can proceed with a substantial cross section only to high excitation states, near the breakup

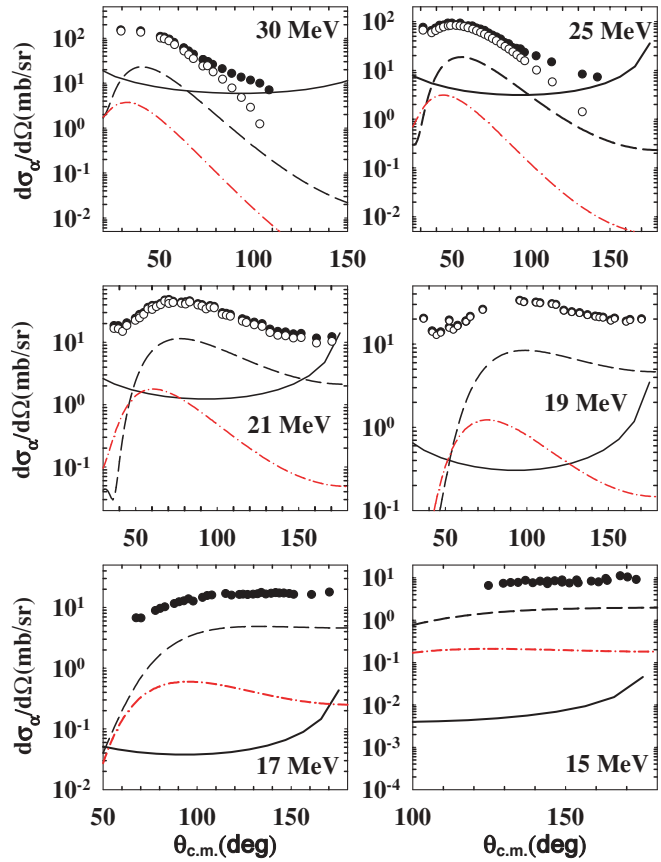

FIG. 3. (Color online) Inclusive α-production cross section for the $^6\text{Li} + ^{90}\text{Zr}$ system near the Coulomb barrier. Filled circles represent the total α cross section, the solid line represents the α coming from the compound reaction, and open circles represent the total minus the compound contribution. The dashed line represents the angular distribution owing to n transfer and the dash-dotted line corresponds to the α group owing to p-transfer reactions according to DWBA calculations (see text for details).

threshold of $^{92}\text{Nb} \rightarrow {}^{90}\text{Zr} + d$. As the discrete states in this region are not known, no attempts have been made to speculate further.

Finite-range DWBA calculations for one-neutron and one-proton transfer were performed using the code FRESCO [33]. The optical potential used in the calculation was composed of two parts, a bare potential and a dynamic polarization potential (DPP) caused by the breakup couplings. The bare potential was derived from the cluster-target empirical optical potential by means of the cluster-folding method; the DPP potential was generated by the coupling of the breakup channel in a CDCC calculation, according to the method described in Refs. [33] and [34] (details on the breakup calculations are presented in our previous work [25] and breakup cross sections are listed in Table I). The same optical-model potential was used for both the entrance and the exit channels. Bound-state wave functions were generated using the Woods-Saxon potentials and with the geometric parameters $r_0 = 1.25$ fm and $a = 0.65$ fm, with the depths of the potentials adjusted to give the correct separation energies. For one-neutron transfer, we have considered states below 4 MeV in the final nucleus ^{91}Zr. The spectroscopic

factors for $^{6}\mathrm{Li} = {}^{5}\mathrm{Li} + n$ were taken from the shell-model prediction [35]. For the states in the final nucleus, the quantum numbers and spectroscopic factors were taken from (d,p) studies [36]. The calculated cross sections for all excited states of ^{91}Zr were summed to get the total n-transfer cross section. Similar calculations were performed for one-proton transfer reactions leading to states in the ^{91}Nb nucleus. We have considered states with only high spectroscopic factors. Spectroscopic factors for $^{6}\mathrm{Li} = {}^{5}\mathrm{He} + p$ were taken from the shell-model predictions [35]. For the states in the final nucleus, quantum numbers and spectroscopic factors were taken from (^{3}He,d) studies [36]. The n-transfer and p-transfer cross sections are presented in Fig. 3, assuming that they lead to the α production in the final state. The integrated cross sections of these transfer channels at different energies are also reported in Table I.

VI. DISCUSSION

We have measured the inclusive α-production cross section at energies around the Coulomb barrier. The measurements show that at lower energies the α-production cross sections approach the reaction cross sections obtained from the elastic scattering measurements. One of the most challenging tasks is to disentangle different reaction channels contributing to the total α production. The statistical model calculations performed for the compound nuclear reaction contributing to α production show that it accounts for a small fraction of the total α production. The compound nuclear contribution decreases toward the barrier energies and is almost negligible below the Coulomb barrier. The estimated breakup cross section using the CDCC calculations amounts to 10% of the total α cross section at higher energies where contributions from all the other channels are significant. Similar predictions have been made about breakup cross sections in earlier exclusive and inclusive measurements [5,13,23,29,37]. In Refs. [26] and [29], it was observed that the total exclusive cross section ($\alpha + d$ and $\alpha + p$) is much smaller compared to the total α-production cross section.

One-neutron and one-proton transfer calculations have been carried out in the DWBA framework to estimate their contribution to α production. These cross sections are also less compared to the total α-production cross sections, although the shapes of the angular distributions are well reproduced by the calculations. The calculated cross section for n transfer are lower by a factor of 6 to 4, from the highest (30 MeV) to the lowest (15 MeV) energy, compared to the inclusive α cross sections. Experimental measurements of the transfer channels in coincidence will be required to test the validity of the calculated transfer results more accurately. The sum of all these channel (breakup and transfer) cross sections, amounting to the α production, is significantly less (<50%) compared to the total α-production cross sections above barrier energies.

We have compared the energy dependence of the total α production owing to the direct and compound reaction mechanisms (see Fig. 4). The contribution from the compound reaction decreases exponentially toward the Coulomb barrier and the direct part (transfer and breakup) increases close to the barrier energies. More experimental data are required to draw a systematic picture of these processes.

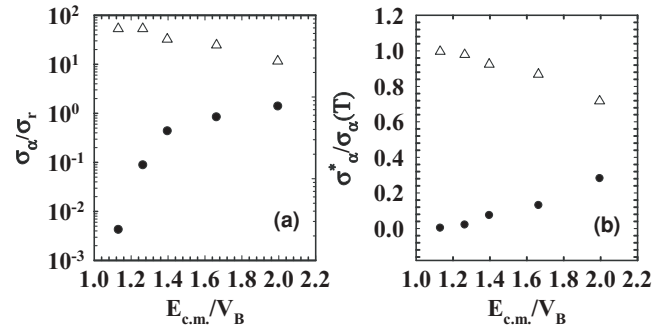

FIG. 4. (a) The direct (open triangles) and compound (filled circles) parts of the α-production cross section relative to the reaction cross section. (b) Ratio of the direct (open triangles) and compound (filled circles) parts of the α-production cross section to the total α-production cross section.

The measured total α cross sections for $^{6}\mathrm{Li} + {}^{90}\mathrm{Zr}$ are compared with the cross sections for other systems, $^{6}\mathrm{Li} + {}^{28}\mathrm{Si}$ [12], $^{6}\mathrm{Li} + {}^{59}\mathrm{Co}$ [37], $^{6}\mathrm{Li} + {}^{58}\mathrm{Ni}$, $^{6}\mathrm{Li} + {}^{118}\mathrm{Sn}$, $^{6}\mathrm{Li} + {}^{120}\mathrm{Sn}$ [38], and $^{6}\mathrm{Li} + {}^{208}\mathrm{Pb}$ [27,39], in Fig. 5. The total α production for the $^{6}\mathrm{Li} + {}^{90}\mathrm{Zr}$ system follows a universal behavior as predicted previously [12]. The experimental Coulomb barriers are taken from Ref. [12]. The Coulomb barrier used for the $^{6}\mathrm{Li} + {}^{90}\mathrm{Zr}$ system is 14.1 MeV. The α cross sections are compared with the difference in the reaction cross sections and fusion cross sections to show the dominance of the α-channel contributions. The reaction cross sections were derived from elastic scattering measurements [25]. The fusion cross sections were obtained by the barrier penetration method using the effective potential derived from CDCC calculations. The α cross sections indicate the dominance of inclusive

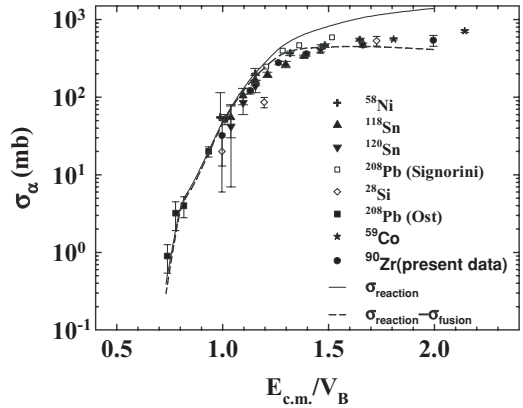

FIG. 5. Total α-production cross section as a function of the projectile energy divided by the Coulomb barrier for ^{6}Li on various targets. ^{28}Si [12], ^{59}Co [37], ^{58}Ni, ^{118}Sn, ^{120}Sn [38], and ^{208}Pb [27,39] are designated by open diamonds, stars, plus signs, upward- and downward-pointing triangles, and filled and open squares, respectively. Present measurements of ^{6}Li on ^{90}Zr are designated by filled circles, which reproduce the universal curve. The reaction and reaction-minus-fusion cross sections for the $^{6}\mathrm{Li} + {}^{90}\mathrm{Zr}$ system are represented by solid and dashed lines, respectively.

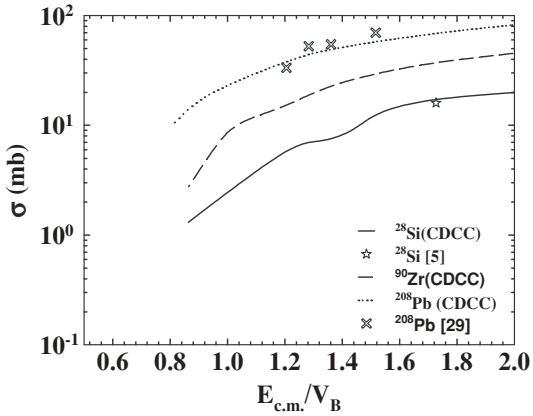

FIG. 6. A comparison of experimental and CDCC-calculated breakup ($\alpha + d$) cross sections as a function of the projectile energy divided by the Coulomb barrier energy for ^{6}Li on various targets: ^{28}Si [5], ^{90}Zr, and ^{208}Pb [29]. CDCC-calculated cross sections for ^{28}Si, ^{90}Zr, and ^{208}Pb are designated by solid, dashed, and dotted lines respectively. Experimental data are denoted by the open star and crosses for ^{28}Si, and ^{208}Pb targets, respectively.

α production at near-barrier energies, although more measurements are required to disentangle the direct- and compound-channel contributions.

We have investigated the target dependence of the calculated exclusive ($\alpha + d$) breakup cross sections for different systems (^{6}Li + ^{28}Si, ^{90}Zr, and ^{208}Pb) in the CDCC framework. The exclusive breakup cross sections from CDCC calculations are compared with the available experimental data [5,29] as shown in Fig. 6. The breakup cross sections calculated by CDCC are in good agreement with the experimental data. Although a universal behavior is observed for the inclusive α-production cross sections, the breakup cross sections show a relatively stronger target mass dependence.

VII. CONCLUSIONS

In summary, we have measured the inclusive α-production cross section for the ^{6}Li + ^{90}Zr system around the Coulomb barrier energies over a wide angular range. Statistical-model and DWBA calculations were performed to disentangle the α contributions owing to the compound and the direct reaction mechanisms. A universal behavior of the α-production cross section is observed, with no target mass dependence, although breakup shows a stronger target mass dependence. DWBA calculations for *n*- and *p*-transfer reactions predict the qualitative feature well, although the quantitative results need to be compared with the measurements of exclusive transfer cross sections. The transfer reactions seem to be more dominant near barrier energies, and breakup cross sections are marginally less compared to reaction cross sections.

ACKNOWLEDGMENTS

The authors thank the BARC/TIFR Pelletron staff for excellent delivery of the beam and the Research Centre, Jülich, for providing the enriched ^{90}Zr target.

[1] M. Dasgupta *et al.*, Phys. Rev. Lett. **82**, 1395 (1999).
[2] V. Tripathi, A. Navin, K. Mahata, K. Ramachandran, A. Chatterjee, and S. Kailas, Phys. Rev. Lett. **88**, 172701 (2002).
[3] A. Mukherjee *et al.*, Phys. Lett. B **636**, 91 (2006).
[4] P. R. S. Gomes, J. Lubian, I. Padron, and R. M. Anjos, Phys. Rev. C **71**, 017601 (2005).
[5] A. Pakou *et al.*, Phys. Lett. B **633**, 691 (2006).
[6] P. K. Rath *et al.*, Phys. Rev. C **79**, 051601(R) (2009).
[7] C. Mahaux *et al.*, Nucl. Phys. A **449**, 354 (1986).
[8] N. Kelley *et al.*, Nucl. Phys. A **571**, 326 (1994).
[9] M. A. Tiede, D. E. Trcka, and K. W. Kemper, Phys. Rev. C **44**, 1698 (1991).
[10] A. M. M. Maciel *et al.*, Phys. Rev. C **59**, 2103 (1999).
[11] A. Pakou *et al.*, Phys. Lett. B **556**, 21 (2003).
[12] A. Pakou *et al.*, Phys. Rev. Lett. **90**, 202701 (2003).
[13] A. Pakou *et al.*, Phys. Rev. C **69**, 054602 (2004).
[14] P. R. S. Gomes *et al.*, Phys. Rev. C **71**, 034608 (2005).
[15] J. O. F. Niello *et al.*, Nucl. Phys. A **787**, 484c (2007).
[16] F. A. Souza *et al.*, Phys. Rev. C **75**, 044601 (2007).
[17] I. Martel *et al.*, Nucl. Phys. A **582**, 357 (1995).
[18] C. Signorini *et al.*, Phys. Rev. C **61**, 061603(R) (2000).
[19] Y. Sakuragi, Phys. Rev. C **35**, 2161 (1987).
[20] J. Takahashi *et al.*, Phys. Rev. Lett. **78**, 30 (1997).
[21] K. Hagino, A. Vitturi, C. H. Dasso, and S. M. Lenzi, Phys. Rev. C **61**, 037602 (2000).
[22] R. S. Mackintosh and N. Keeley, Phys. Rev. C **70**, 024604 (2004).
[23] C. Beck, N. Keeley, and A. Diaz-Torres, Phys. Rev. C **75**, 054605 (2007).
[24] N. Takigawa and H. Sagawa, Phys. Lett. B **265**, 23 (1991).
[25] H. Kumawat *et al.*, Phys. Rev. C **78**, 044617 (2008).
[26] S. Santra *et al.*, Phys. Lett. B **677**, 139 (2009).
[27] C. Signorini *et al.*, Eur. Phys. J. A **10**, 249 (2001).
[28] E. F. Aguilera *et al.*, Phys. Rev. Lett. **84**, 5058 (2000).
[29] C. Signorini *et al.*, Phys. Rev. C **67**, 044607 (2003).
[30] A. Shrivastava *et al.*, Phys. Lett. B **633**, 463 (2006).
[31] A. Gavron, Phys. Rev. C **21**, 230 (1980).
[32] A. V. Ignatyuk, G. N. Smirenkin, and A. S. Tishin, Sov. J. Nucl. Phys. **21**, 255 (1975).
[33] I. J. Thompson, Comput. Phys. Rep. **7**, 167 (1988).
[34] I. J. Thompson, FRESCO (May 2007), version FRES 2.3.
[35] S. Cohen and D. Kurath, Nucl. Phys. A **101**, 1 (1967).
[36] C. R. Bingham and M. L. Halbert, Phys. Rev. C **2**, 2297 (1970).
[37] F. A. Souza *et al.*, Nucl. Phys. A **821**, 36 (2009).
[38] K. O. Pfeiffer, E. Speth, and K. Bethge, Nucl. Phys. A **206**, 545 (1973).
[39] R. Ost, E. Speth, K. O. Pfeiffer, and K. Bethge, Phys. Rev. C **5**, 1835 (1972).